Mechanism of Hydrogen Storage on Fe3B

Article *in* Chemical Communications · October 2020

DOI: 10.1039/D0CC03741A

7 authors, including:

Zhao Ding
Illinois Institute of Technology
34 PUBLICATIONS **509** CITATIONS

SEE PROFILE

Weijie Yang
North China Electric Power University
60 PUBLICATIONS **860** CITATIONS

SEE PROFILE

ChemComm

COMMUNICATION

View Article Online
View Journal

Cite this: DOI: 10.1039/d0cc03741a

Mechanism of hydrogen storage on Fe_3B†

Zhao Ding,[ab] Hao Li,[c] Ge Yan,[d] Weijie Yang,*[d] Zhengyang Gao,[d] Wenhui Ma[e] and Leon Shaw[b]

Received 28th May 2020,
Accepted 13th October 2020

DOI: 10.1039/d0cc03741a

rsc.li/chemcomm

Recent experimental finding has indicated that Fe_3B has the capacity to uptake and release hydrogen. However, the mechanism has not been clarified. Here, for the first time, the characteristics were investigated through the electronic structures and energies of H_2 molecules adsorbed on Fe_3B using density functional theory calculations. Most importantly, this work provides a guideline for experimental investigation of wide-source and low-cost Fe-based hydrogen storage materials.

The growing awareness of environmental pollution caused by the burning of conventional fossil fuel has motivated a large number of studies on renewable hydrogen fuel sources. Meanwhile, plenty of studies have been focused on the discovery and synthesis of solid-state materials for onboard hydrogen storage, due to its advantages of high hydrogen storage density, moderate working pressure, and good safety performance, compared to compressed gaseous and cryogenic liquid hydrogen technologies.[1,2] However, no material so far has met the expectations of industrial standards of on-board hydrogen storage systems (which release and uptake 7.5 wt% H_2 at a temperature of 95–105 °C).[3,4]

Lately, our group has devised a novel process with high-energy ball milling (BM) of MgH_2 at ambient temperature in conjunction with aerosol spraying (AS) of $LiBH_4$ dissolved in tetrahydrofuran (THF) solution.[5–10] Through the BMAS process, we have shown that the reversible hydrogen storage capacity of the $LiBH_4 + MgH_2$ mixture can reach as high as ~4.11 wt% in the solid state without any catalyst, and $Mg(BH_4)_2$ is formed *via* the direct reaction between MgH_2 and $LiBH_4$ for the first time as expressed in reaction (1).[5,7] Fe comes from the wear of stainless steel balls during ball milling, which would react with B that comes from the gradual decomposition of $Mg(BH_4)_2$ *via* reaction (2), to form Fe_3B, as shown in reaction (3). The formation of Fe_3B has been ascribed to an interesting phenomenon wherein the amount of hydrogen uptake in hydrogenation is higher than the hydrogen released in the previous dehydrogenation (starting from the second cycle).[5] The hydrogen amount of desorption and adsorption as a function of dehydrogenation and re-hydrogenation cycles was plotted in a histogram as shown in Fig. S1 (ESI†).[5]

$$2LiBH_4(s) + MgH_2(s) = Mg(BH_4)_2(s) + 2LiH(s) \quad (1)$$

$$Mg(BH_4)_2(s) \rightarrow MgH_2(s) + 2B(s) + 3H_2(g) \quad (2)$$

$$3Fe(s) + B(s) = Fe_3B(s) \quad (3)$$

Note that the self- and acroscopic diffusion of the hydrogen atom in amorphous Fe_3B has been studied with first-principles calculations.[11,12] However, to the best of our knowledge, there is currently no report on the interaction between Fe_3B and H_2 for hydrogen storage. Xie and Gu[13] reported that H_2 could dissociate and interact with iron on Fe(110), forming stable Fe–H bonds. Pozzo and Alfè[14] further confirmed that theoretically doping Fe on a Mg(0001) surface results in facile H_2 dissociation at the Fe site, due to the very low dissociation barrier. Besides, many studies[15–20] have shown that hydrides can be formed easily at Fe-related sites, so it is not groundless to consider Fe-related materials such as Fe_3B as a new type of hydrogen storage material.

In this study, for the first time, the mechanism of H_2 adsorption and desorption on Fe_3B was investigated using density functional theory (DFT) calculations. Firstly, the geometric structures of the Fe_3B model and the adsorption characteristics

[a] The State Key Laboratory of Refractories and Metallurgy, Institute of Advanced Materials and Nanotechnology, Wuhan University of Science and Technology, Wuhan, China
[b] Department of Mechanical, Materials and Aerospace Engineering, Illinois Institute of Technology, Chicago, Illinois, USA
[c] Department of Physics, Technical University of Denmark, Kongens, Lyngby 2800, Denmark
[d] School of Energy, Power and Mechanical Engineering, North China Electric Power University, Baoding, China. E-mail: yangwj@ncepu.edu.cn
[e] Faculty of Metallurgical and Energy Engineering, Kunming University of Science and Technology, Kunming, China

† Electronic supplementary information (ESI) available. See DOI: 10.1039/d0cc03741a

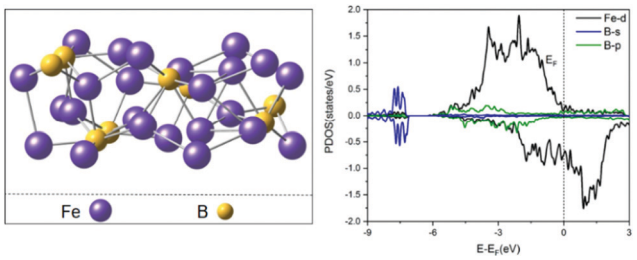

Fig. 1 Optimized geometric structure and the PDOS plot of Fe_3B.

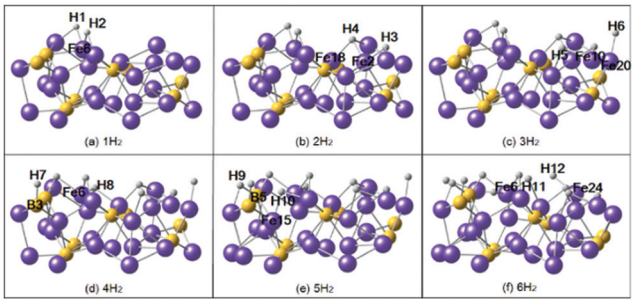

Fig. 2 Optimized geometric structures of nH_2 (n = 1–6) adsorbed on Fe_3B. The purple, orange, and gray spheres represent Fe, B, and H atoms, respectively.

of H_2 on Fe_3B were studied through the analysis of adsorption configurations and adsorption energies. Secondly, the adsorption mechanism of H_2 on Fe_3B was investigated through the calculated electron density difference (EDD), projected density of states (PDOS), and electron localization function (ELF). Finally, thermodynamic analysis and *ab initio* molecular dynamics (AIMD) simulations were adopted to study the dehydrogenation characteristics of Fe_3B. This work provides an understanding of the hydrogenation and dehydrogenation over the Fe_3B surface, so as to design similar Fe-based compounds as a viable system for reversible hydrogen storage applications near ambient temperature.

The Fe_3B structures were modelled in the form of an orthorhombic crystal, consisting of 24 Fe and 8 B atoms, with lattice parameters of a = 9.70, b = 7.01, and c = 4.23. Fig. 1 shows a stereogram of the stable crystal structure. To understand the binding mechanism between Fe and B, the PDOS of Fe_3B was calculated (Fig. 1). The d orbital of Fe is asymmetric with two spin states, which indicates that the system is magnetic. The calculated average magnetic moment of Fe_3B is 1.70 μB, which is significantly larger than that of FeB (1.13 μ_B).[21] Furthermore, the d orbital of Fe hybridizes with the p orbital of B mainly in an energy range from −3 to 3 eV. Such a phenomenon is consistent with the work of Zhang *et al.*[22] These hybridizations play important roles to form a strong Fe–B bond, leading to a rational Fe_3B system that is sufficiently stable to achieve the process of H_2 adsorption.

Based on the modelled Fe_3B structure, potential adsorption sites and different orientations of H_2 were calculated to obtain the most stable adsorption configurations, as shown in Fig. 2. The corresponding adsorption energy, charge variation, and bond length are listed in Table S1 (ESI†).

As shown in Fig. 2a, the first H_2 is adsorbed at the Fe site, with an adsorption energy of −1.00 eV. Such strong chemisorption is accompanied by the dissociation of H_2, with the H–H elongating to 2.49 Å compared to that of 0.75 Å in the H_2 gas molecule. The distances between H and the nearest Fe are 1.68 and 1.67 Å. Fig. 2b shows the possible adsorption sites that are explored on the basis of Fig. 2a, achieving a stable configuration for the second H_2 adsorption on Fe_3B, with an adsorption energy of −1.17 eV. It should be noted that this H_2 dissociates more facile than the first H_2. Similarly, the configurations of Fe_3B with the adsorption of the third to sixth H_2 molecules were also optimized (Fig. 2c–f). The adsorption energy is increasing from the first H_2 to the third H_2 at the Fe sites. Fig. 2c shows the maximum adsorption energy of −1.19 eV with a hydrogen coverage of 0.5 on Fe_3B. In terms of the fourth and fifth H_2, H coverage started to be adsorbed at the B sites rather than the Fe sites. Meanwhile, the adsorption energy decreases from the adsorption of the fourth H_2 to the sixth H_2. It should be noted that the six H_2 molecules are all adsorbed on the five Fe atoms on the top layer as shown in Fig. 2, which indicates a corresponding hydrogen storage capacity of 4.15 wt% at the surface. Though the adsorption energies in these three models are relatively weak, all the H_2 molecules dissociate in all six adsorption models. In comparison, Liu *et al.*[23] studied six H_2 adsorptions on Ti-decorated B38 fullerene with the maximum adsorption energies of 0.45 eV, which shows much inferior H_2 adsorption ability than that of Fe_3B investigated in this work.

Then, we performed further research to compare the hydrogenation capacity between the defective and perfect models of the 1H2 system. The Fe6 vacancy and its nearest two vacancies (Fe8 vacancy and Fe22 vacancy) were studied (Fig. S2, ESI†). Our results showed that the adsorption energies of the Fe6 vacancy structure shown in Fig. S2(a) (ESI†) and the Fe8 vacancy structure shown in Fig. S2(b) (ESI†) are −1.00 and −1.02 eV, respectively, being similar to that of the perfect model (−1.00 eV). The Fe22 vacancy structure shown in Fig. S2(c) (ESI†) has a value of −0.32 eV, much smaller than that of the perfect model. The charge changes of the adsorption sites in the perfect and defective models were further investigated, as shown in Table S2 (ESI†). In the model with Fe6 vacancy, B5 has the most negative charge changes, indicating more facile hydrogen desorption. In the model with Fe8 vacancy, Fe6 loses the most charge. However, the model with Fe22 vacancy has weak hydrogen adsorption capacity with small H–H elongation. Fe6 obtained 0.12 e, resulting in weak adsorption capacity. In conclusion, it is expected that the defect sites of Fe_3B have less significant improvement in hydrogen adsorption.

To further understand the adsorption properties of H_2 onto Fe_3B, the relevant charge, electronic, and bonding properties are analyzed by EDD, PDOS, and ELF.

EDD is used as a subtle tool to highlight the bonding mechanism in the process of adsorption. The Bader charge changes of the first to sixth H_2 molecules and the substrates are summarized in Table S1 (ESI†), revealing that H_2 always gains electrons from the substrates during hydrogen adsorption.

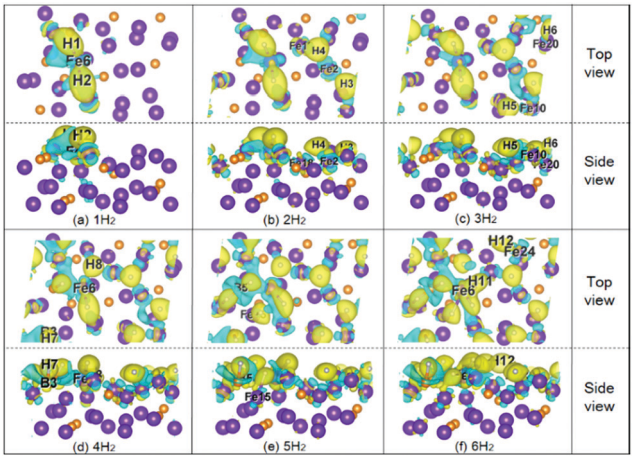

Fig. 3 EDD maps of the first to sixth H_2 adsorbed on Fe_3B. The cyan and yellow regions represent electron loss and gain, respectively.

With more negative energies, the adsorption systems of the fifth and sixth H_2 would have less electron transfer. The specific charge changes of all the hydrogen atoms and adsorption sites in the current hydrogenation process are listed in Table S3 (ESI†). According to the specific charge analysis (Table S3, ESI†), the obvious charge variation difference between Fe and H can show the formation trend of stable ionic bonds which leads to large adsorption energies. Considering the similar charge variation between B and H, there seem to be covalent bonds. To further analyze the charge properties of the first to six H_2 molecule adsorption on Fe_3B, EDD maps at the top and side views are plotted in Fig. 3. The Fe, B, and H atoms are colored in purple, orange, and gray, respectively.

Fig. 3 shows that H_2 is always surrounded by yellow regions, which indicates that there are aggregations of electrons. Fe and B are always surrounded by cyan regions especially at the adsorption site, and the lower-level atoms have almost no electron gain or loss. Fig. 3 further confirms that some charges have transferred from the Fe or B atoms to H which is consistent with our Bader charge analysis. Moreover, the first H_2 has the largest change in the electron gain mainly in (d–f). The adsorption site of the fourth and sixth H_2 is Fe6 which is also the adsorption site of the first H_2, leading the first H_2 to reduce electrons. The obvious reduction in the adsorption energy from the third to the fourth H_2 can be attributed to the following two possibilities. The first reason is that it turns out to be very difficult to transfer electrons from B to H because B exhibits weaker metallicity than Fe. The second reason is that Fe6 has already been occupied by H8, which makes it too saturated to transfer more electrons. Also, the effect of the Fe_3B surface on the H_2 adsorption was analyzed through PDOS, as shown in the section 2 (ESI†).

ELF is used to study different bonding interactions. ELF values are calculated from the excess kinetic energy density due to the Pauli mutual exclusion and the Thomas–Fermi kinetic energy functional.[24] It should be noted that a higher value of ELF stands for a stronger localization region which is better for finding an electron or a pair of localized electrons. For covalent bonding, ELF goes to a large value ranging from 0.6 to 1, while for ionic boning, ELF goes to a small value ranging from 0 to 0.5. The ELF contour maps of the first to sixth H_2 adsorbed on Fe_3B are shown in Fig. 4. Both of the two-dimensional images were calculated from the best plane containing the relevant H_2 adsorption site. The region with strong localization tends to be red, while that with strong delocalization tends to be blue.

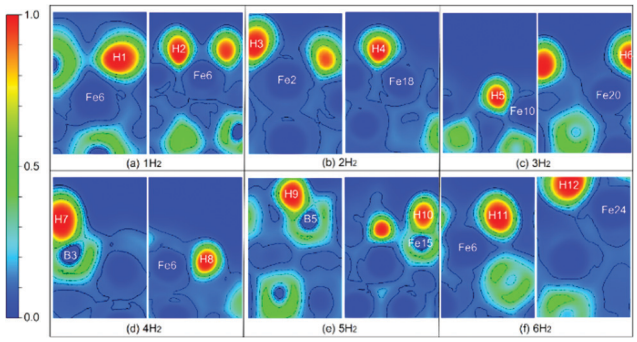

Fig. 4 ELF maps of the first to sixth H_2 adsorbed on Fe_3B.

According to the ELF maps (Fig. 4), the ELF value is close to 1 at the H site, indicating a highly localized electron position. The hydrogen in the gas phase is connected by a highly localized covalent bond, and the degree of electron localization is significantly reduced after full activation. In contrast, the Fe and B sites are highly delocalized since their ELF values are close to zero. These notable differences confirm that Fe_3B donates electrons to H_2. H and Fe/B tend to form ionic bonds because of the relatively low ELF value (0–0.5). The ELF contours of the H atoms in (a–c) are not spherically shaped but polarized to Fe atoms because of the repulsive force between the negatively charged H atoms. This polarization, in turn, reduces the interaction of H_2 thus leading to a shorter H–H bond. The degree of delocalization of the B3 and Fe15 atoms shown in Fig. 4d and 5e is relatively stronger than before, indicating a weak interaction between H_2 and Fe_3B. Therefore, there is a significant decrease in the adsorption energies. The smaller increase of adsorption energy finally can be attributed to the reduced delocalization degree of Fe (Fig. 4f).

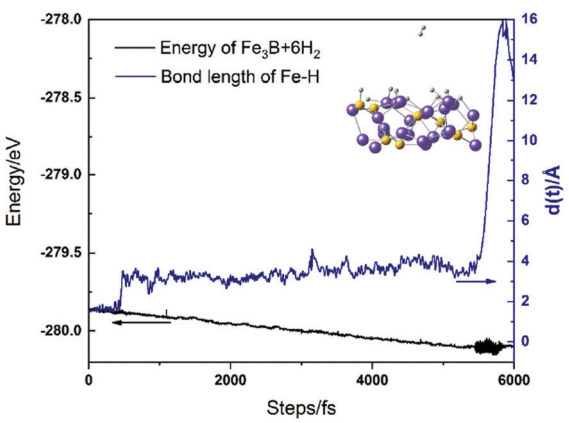

Fig. 5 AIMD profiles of the H_2 desorption on Fe_3B + $6H_2$ at 538 K.

Firstly, as one of the most important parameters of experiments, the effect of the temperature on hydrogen storage should be considered.[25,26] Thermodynamics analysis of the system was conducted for further applications based on the calculation of Gibbs free adsorption energy (ΔG) under different temperatures. The vibrational frequency was calculated through numerical Hessian calculations with finite displacements of $\pm$0.02 Å. In order to evaluate the hydrogen storage capacity, ΔG values of the first to the sixth H_2 adsorption on Fe_3B were plotted ranging from 298.15 to 1000 K (Fig. S5, ESI†). Note that a negative value of ΔG indicates that the adsorption process can occur spontaneously. And the more negative the ΔG value, the stronger the interaction between H_2 and Fe_3B.

It is found that all of the ΔG values increase with the increase of temperature, indicating that temperature has an inhibitory effect on the adsorption. As seen from Fig. S4 (ESI†), it is worth noting that the adsorption order is consistent with the above calculations and analysis. All of the ΔG values of the first, second, and third H_2 adsorption remain negative under a lower temperature range. In contrast, the ΔG values of the fourth, fifth, and sixth H_2 adsorption are mostly positive which indicates that H_2 adsorption is no longer easy to occur at Fe_3B. As expected, the adsorption of the third H_2 is the most favorable reaction under 500 K. Meanwhile, according to Fig. S4 (ESI†), the required conditions for the release of the first, second, third, fourth, fifth, and sixth H_2 are all under the experimental temperature (538 K).

In order to further investigate the dehydrogenation ability and thermal stability of Fe_3B, the desorption kinetics of the adsorbed H_2 on $Fe_3B + 6H_2$ was investigated by AIMD. AIMD simulations were performed using the VASP package, for up to 10 ps with a time step of 1 fs. To be consistent with the experimental conditions, the whole simulation process was also conducted under 538 K. The displacement of hydrogen was measured as the bond length of Fe–H and marked in blue as shown in Fig. 5. As shown, H begins to displace after about 5500 fs of simulation. A peak appears at about 6000 fs, which means the longest displacement with a value of 15.98 Å. According to Fig. 5, the potential energy of $Fe_3B + 6H_2$ (black line) is constantly decreasing until 6000 steps, which shows an equilibrium state shock. The escaped H as shown in Fig. 5 are H1 and H12. They both have smaller charge transfers in the adsorption processes, so they interact with Fe_3B weakly and are easy to be removed. With the AIMD simulation results it can be concluded that Fe_3B has the ability to release H_2 at 538 K, in good agreement with previous experiments.[5] Since Fe is one of the most abundant elements in the Earth's crust, both the origin and cost of Fe-based materials are rather competitive for hydrogen storage when compared to Mg-based materials.

In summary, in this paper, the adsorption characteristics of the first to sixth H_2 on Fe_3B were studied by DFT calculations. Dissociative adsorption is a favorable adsorption type for H_2, resulting in two separate H on Fe_3B. The adsorption energy increases at first and then decreases with a higher H coverage, reaching saturation when the H coverage is 0.5. The Fe sites are more favorable for hydrogen activation and adsorption, compared to the B sites. The interaction type of H_2 on Fe_3B is dominated by ionic bonds which brings about strong adsorption strength. The dehydrogenation performance of Fe_3B at 538 K as calculated here, is in good agreement with the previous experiments.

This work was supported by the U.S. National Science Foundation (NSF) with the Award No. CMMI-1261782, the National Natural Science Foundation of China (No. 52006073), the Beijing Municipal Natural Science Foundation (2182066), the Natural Science Foundation of Hebei Province of China (B2018502067 and E2020502023) and the Fundamental Research Funds for the Central Universities (JB2015RCY03 and 2017XS121).

Conflicts of interest

There are no conflicts to declare.

References

1 Z. Xiong, C. K. Yong, G. Wu, P. Chen, W. Shaw, A. Karkamkar, T. Autrey, M. O. Jones, S. R. Johnson and P. P. Edwards, *Nat. Mater.*, 2008, **7**, 138.
2 P. Chen, Z. Xiong, J. Luo, J. Lin and K. L. Tan, *Nature*, 2002, **420**, 302.
3 Z. Ding, S. Li, Y. Zhou, Z. Chen, W. Yang, W. Ma and L. Shaw, *Nano Mater. Sci.*, 2020, **2**, 109–119.
4 Target Explanation Document: Onboard Hydrogen Storage for Light-Duty Fuel Cell Vehicles, 2017.
5 Z. Ding, H. Li and L. Shaw, *Chem. Eng. J.*, 2020, **385**, 123856.
6 Z. Ding, Y. Lu, L. Li and L. Shaw, *Energy Storage Mater.*, 2019, **20**, 24–35.
7 Z. Ding and L. Shaw, *ACS Sustainable Chem. Eng.*, 2019, **7**, 15064–15072.
8 Z. Ding, P. Wu and L. Shaw, *J. Alloys Compd.*, 2019, **806**, 350–360.
9 Z. Ding, X. Zhao and L. L. Shaw, *J. Power Sources*, 2015, **293**, 236–245.
10 Y. Zhong, X. Wan, Z. Ding and L. L. Shaw, *Int. J. Hydrogen Energy*, 2016, **41**, 22104–22117.
11 S. Hao and D. S. Sholl, *J. Chem. Phys.*, 2009, **130**, 244705.
12 S. Hao, M. Widom and D. S. Sholl, *J. Phys.: Condens. Matter*, 2009, **21**, 115402.
13 W. Xie, L. Peng, D. Peng, F. L. Gu and J. Liu, *Appl. Surf. Sci.*, 2014, **296**, 47–52.
14 M. Pozzo and D. Alfe, *Int. J. Hydrogen Energy*, 2009, **34**, 1922–1930.
15 Y.-C. Liu, K.-T. Chu, R.-L. Jhang, G.-H. Lee and M.-H. Chiang, *Chem. Commun.*, 2013, **49**, 4743–4745.
16 F. Aubertin, U. Gonser and S. Campbell, *J. Phys. F: Met. Phys.*, 1984, **14**, 2213.
17 J. I. van der Vlugt, T. B. Rauchfuss, C. M. Whaley and S. R. Wilson, *J. Am. Chem. Soc.*, 2005, **127**, 16012–16013.
18 D. Papaconstantopoulos and A. Switendick, *J. Less-Common Met.*, 1982, **88**, 273–281.
19 J. Xu, A. Avellan, H. Li, X. Liu and G. V. Lowry, *Adv. Mater.*, 2020, 1906910.
20 Z. Cao, H. Li, X. Xu and J. Xu, *Chem. Eng. J.*, 2020, 124876.
21 A. Gueddouh, B. Bentria, I. K. Lefkaier and Y. Bourourou, *Bull. Mater. Sci.*, 2016, **39**, 1427–1434.
22 W. H. Zhang, Z. Q. Lv, Z. P. Shi, S. H. Sun, Z. H. Wang and W. T. Fu, *J. Magn. Magn. Mater.*, 2012, **324**, 2271–2276.
23 P. Liu, H. Zhang, X. Cheng and Y. Tang, *Int. J. Hydrogen Energy*, 2016, **41**, 19123–19128.
24 J. Santos, W. Tiznado, R. Contreras and P. Fuentealba, *J. Chem. Phys.*, 2004, **120**, 1670–1673.
25 Z. Ding, Z. Chen, T. Ma, C.-T. Lu, W. Ma and L. Shaw, *Energy Storage Mater.*, 2020, **27**, 466–477.
26 H. Li, S. Xu, M. Wang, Z. Chen, F. Ji, K. Cheng, Z. Gao, Z. Ding and W. Yang, *J. Mater. Chem. A*, 2020, **8**, 17987–17997.

